Analysis of the Mode-Specific Excited-State Energy Distribution and Wavelength-Dependent Photoreaction Quantum Yield in Rhodopsin

Judy E. Kim, Michael J. Tauber, and Richard A. Mathies
Department of Chemistry, University of California at Berkeley, Berkeley, California 94720 USA

ABSTRACT The photoreaction quantum yield of rhodopsin is wavelength dependent: $\phi(\lambda)$ is reduced by up to 5% at wavelengths to the red of 500 nm but is invariant ($\phi = 0.65 \pm 0.01$) between 450 and 500 nm (Kim et al., 2001). To understand this nonstatistical internal conversion process, these results are compared with predictions of a Landau-Zener model for dynamic curve crossing. The initial distribution of excess photon energy in the 28 Franck-Condon active vibrational modes of rhodopsin is defined by a fully thermalized sum-over-states vibronic calculation. This calculation reveals that absorption by high-frequency unreactive modes (e.g., C=C stretches) increases as the excitation wavelength is shifted from 570 to 450 nm whereas relatively less energy is deposited into reactive low-frequency modes. This result qualitatively explains the experimentally observed wavelength dependence of $\phi(\lambda)$ for rhodopsin and reveals the importance of delocalized, torsional modes in the reactive pathway.

INTRODUCTION

Wald's discovery that a *cis*-to-*trans* isomerization of 11-*cis* retinal constitutes the photochemical basis of vision (Wald, 1968) has inspired a wide variety of experiments to understand the mechanism of this reaction in rhodopsin (Sakmar et al., 2002; Mathies and Lugtenburg, 2000; Mathies, 1999; Kochendoerfer and Mathies, 1995). Dramatic differences in the speed and isomerization quantum yield of the protein-bound 11-*cis* retinal protonated Schiff base (Schoenlein et al., 1993; Dartnall, 1968) compared to solution (Kandori et al., 1995; Becker and Freedman, 1985) emphasize the unique nature of the excited-state dynamics resulting from protein-chromophore interactions. Specifically, the ultrafast product formation time of 200 fs (Schoenlein et al., 1993) and the observation of coherent vibrational oscillations in the absorption of the impulsively produced photoproduct (Wang et al., 1994) indicate that the photochemistry occurs from nonstationary vibronic states. In addition, the fact that the photoreaction occurs before statistical randomization of energy (Kim and Mathies, 2002) indicates that altering the initial preparation of the excited-state wavepacket should influence the photochemical outcome. This nonstationary vibronic state model for the photochemistry of vision thus motivates our experimental and computational studies of photoproduct formation as a function of excitation wavelength.

The classification of a reaction as statistical or nonergodic was developed primarily through studies of gas-phase unimolecular reactions. A founding theory is that of Rice-Ramsperger-Kassel-Marcus (RRKM) in which the central assumption is that the rate of energy randomization is much faster than chemical reaction (Frost, 1973). Non-RRKM behavior may arise due to a ''bottleneck'' in phase space (intrinsic non-RRKM) or as a result of an ultrafast reaction rate that prevents the statistical redistribution of internal energy before product formation (apparent non-RRKM) (Bunker and Hase, 1973). Although there are many reports of apparent non-RRKM behavior for gas-phase unimolecular reactions (Lee et al., 2000; Diau et al., 1998; Syage et al., 1984; Kim et al., 1996), very few examples of non-RRKM behavior have been reported for condensed-phase reactions. Given the enhanced rate of intramolecular vibrational energy redistribution (IVR) in condensed phase due to solvent-induced fluctuations of solute levels as well as direct coupling between solute and solvent modes (Bakker, 1993), it is generally thought that S_1 IVR rates in liquids are much faster than internal conversion rates. One unique example is *trans*-stilbene in which the gas-phase reaction exhibits non-RRKM behavior whereas the condensed phase isomerization is consistent with RRKM theory (Syage et al., 1984).

Although there has been no direct comparison between the reaction rate for isomerization calculated using RRKM theory and the experimental product formation time of 200 fs, the 50-fs excited-state lifetime of rhodopsin (Kochendoerfer and Mathies, 1996) is comparable to or shorter than typical IVR times of large condensed-phase, polyatomic molecules (Elsaesser and Kaiser, 1991). Therefore, the isomerization of the 11-*cis* retinal chromophore in rhodopsin likely follows a nonergodic pathway. The unthermalized nature of the reaction requires a dynamic model such as that presented by Landau and Zener (Landau, 1932; Zener, 1932; Syage et al., 1984) where the reaction quantum yield depends on the velocity of nuclear motion in the crossing region (Fig. 1) as expressed by the equation $\phi = e^{-k/\nu}$, where ν is the wavepacket velocity that depends on excess energy, and k reflects the energy difference and shapes of the potential energy surfaces. Therefore, the quantum yield should depend on the excitation energy or ν. A more sophisticated, multidimensional picture of the isomerization reaction has also been developed that involves a dynamic

Submitted October 7, 2002, and accepted for publication November 26, 2002.

Address reprint requests to Richard A. Mathies, Fax: 510-642-3599; E-mail: rich@zinc.cchem.berkeley.edu.

0006-3495/03/04/2492/10 $2.00

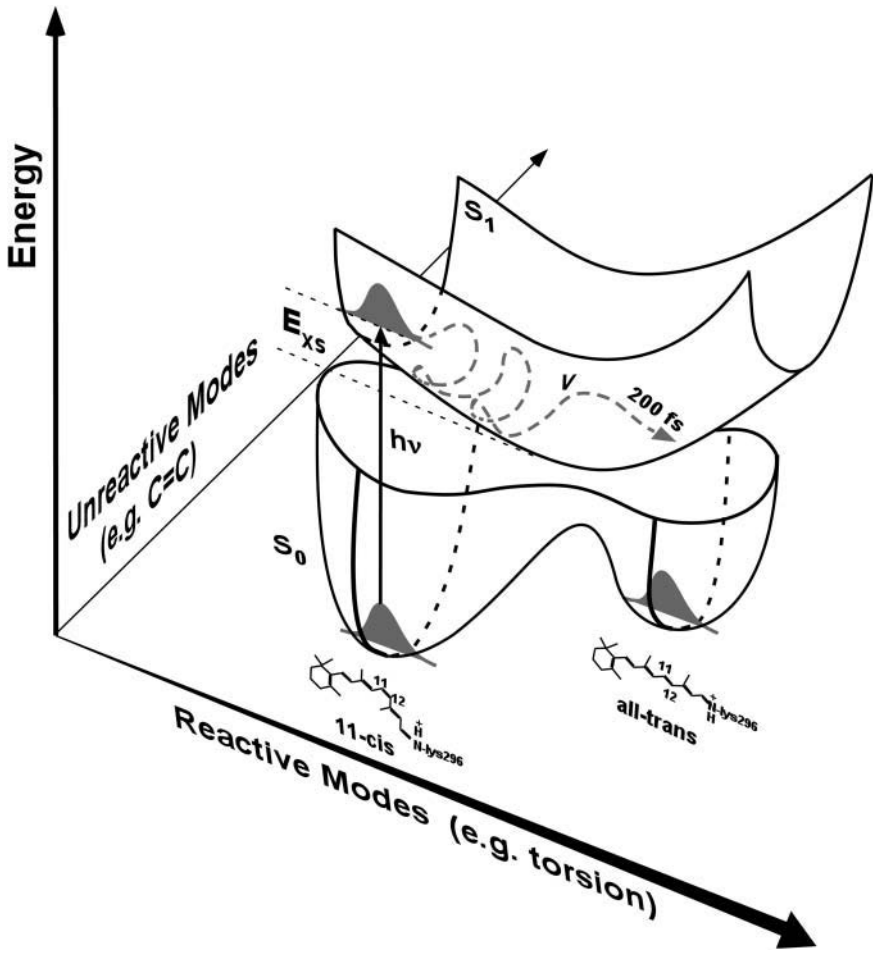

FIGURE 1 Schematic two-dimensional potential energy surface for rhodopsin photoisomerization illustrating reactive and unreactive degrees of freedom. After photon absorption, excess energy (E_{xs}) remains localized within the Franck-Condon active modes, and the distribution of this energy between reactive and unreactive vibrational modes is strongly dependent on excitation wavelength. The excited-state wavepacket rapidly evolves along S_1, and crosses to the ground-state product well with velocity v. The probability for curve crossing, ϕ, depends on the velocity via $\phi_\lambda = e^{-k/v}$. Excess energy deposited in reactive degrees of freedom results in an increased wavepacket velocity along the reaction coordinate and hence, a greater probability for curve crossing.

passage of the wavepacket through a conical intersection (Garavelli et al., 1999a; Garavelli et al., 1998; Vreven et al., 1997; Ben-Nun and Martinez, 1998; Molnar et al., 2000).

Our initial goal was to probe the mode-specific reaction dynamics of rhodopsin by experimental measurement of the dependence of the reaction quantum yield on excitation wavelength (Kim et al., 2001). This work revealed a wavelength-dependent reaction quantum yield between 500 and 570 nm, and a constant quantum yield of 0.65 $\pm$ 0.01 between 450 and 500 nm, as shown in Fig. 2. The value of $\phi_{500} = 0.65 \pm 0.01$ is the most accurate result to date and falls well within the errors of the previous measurements (Dartnall, 1968; Hurley et al., 1977). To more thoroughly understand these results, we present here a complete Franck-Condon analysis of the distribution of excess energy after photoexcitation based on results from resonance Raman intensity analysis (Loppnow and Mathies, 1988; Lin et al., 1998). The resulting knowledge of the wavelength-dependent mode-specific distribution of excess energy in the excited state allows us to quantitatively predict $\phi(\lambda)$ using a one-dimensional Landau-Zener (LZ) picture. In addition to testing the extent to which the LZ picture is valid, this comparison between observed and predicted $\phi(\lambda)$ provides us with insight regarding the origin of the wavelength dependence of the isomerization reaction quantum yield. Our results provide a deeper understanding of visual photochemistry by elucidating the contribution of reactive and unreactive degrees of freedom to the absorption, and by revealing how the initial preparation of the excited-state wavepacket affects the photochemical outcome in this nonergodic reaction.

MATERIALS AND METHODS

The methods used for the measurement of relative quantum yields of rhodopsin have been described in detail elsewhere (Kim et al., 2001). Here, we only describe our computational method for analyzing the excited-state Franck-Condon (FC) energy distributions. The absorption spectrum was computed from sums of Franck-Condon factors (Lax, 1952) to determine the contribution of each Franck-Condon active mode to the absorption cross section at a specific excitation wavelength. In this sum-over-states model, the ground and excited state surfaces are assumed to be harmonic and differ from each other only in their equilibrium positions. A set of N normal modes can then be treated as a collection of N independent harmonic oscillators as shown in Fig. 3, and the multidimensional FC factors can be written as products of one-dimensional overlaps. The fully thermalized absorption cross section can then be written as (Myers and Mathies, 1987)

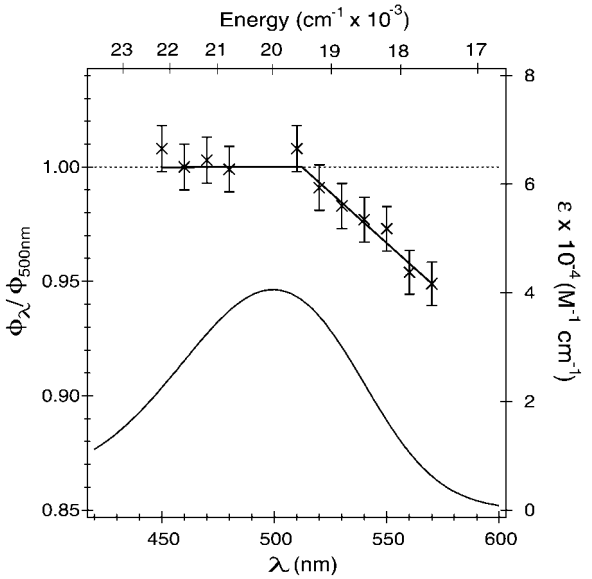

FIGURE 2 Summary of results for the wavelength dependence of the quantum yield of rhodopsin (Kim et al., 2001). The linear fit to the quantum yield data is added as a guide. Errors are reported as $\pm 1\sigma$. The experimental absorption spectrum for rhodopsin is also displayed (*solid curve*, *right axis*).

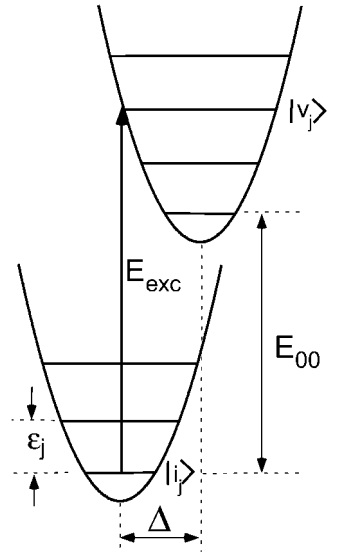

FIGURE 3 Schematic diagram of Franck-Condon absorption process for a single vibrational degree of freedom, mode *j*. The incoming photon has energy E_{exc}. Vibrational levels in the ground and excited state have frequency ε_j and are denoted $|i_j\rangle$ and $|v_j\rangle$, respectively. The harmonic surfaces are displaced by a dimensionless parameter Δ and the energy difference between the lowest vibrational ground- and excited-state levels is E_{00}.

$$\sigma_A(E_{exc}) = \frac{4\pi e^2 M^2 E_{exc}\Gamma_L}{3\hbar cnW}\int_0^\infty \exp\left[\frac{-(E-E_{00})^2}{2\theta_{inh}^2}\right]dE \times \sum_{i_1}\cdots\sum_{i_N}\prod_{j=1}^{N} B_{i_j}\sum_{\nu_1}\cdots\sum_{\nu_N}\frac{\prod_{j=1}^{N}|\langle\nu_j|i_j\rangle|^2}{\left[\sum_{j=1}^{N}\varepsilon_j(\nu_j - i_j) + E_{00} - E_{exc}\right]^2 + \Gamma_L^2}, \quad (1)$$

where M is the electronic transition length (Å), n is the solution index of refraction, Γ_L is a Lorentzian halfwidth at half maximum (HWHM) of the homogeneous linewidth (cm^{-1}), E_{00} is the average 0-0 energy (cm^{-1}), θ_{inh} is the Gaussian standard deviation for inhomogeneous site broadening (cm^{-1}), B_{i_j} is the Boltzmann factor for mode j in level i, W is a normalization factor when inhomogenous broadening is utilized ($= \theta_{inh}\sqrt{2\pi}$), ε_j is the vibrational energy for mode j (cm^{-1}), ν_j is the excited-state level and i_j is the ground-state level for mode j. The Boltzmann term B_{i_j} is given as:

$$B_{i_j} = \left(1 - e^{-\varepsilon_j/kT}\right)\cdot e^{-i_j\varepsilon_j/kT} \quad (2)$$

and reflects the fraction of molecules in the i^{th} vibrational state of mode j at temperature T. The FC factors $|\langle\nu_j|i_j\rangle|^2$ have been derived for the general harmonic case (Manneback, 1951), and we use the recursion relations in the case of equal ground and excited-state frequencies (Myers and Mathies, 1987).

To quantitatively determine how energy is distributed among the FC active modes at various excitation energies, it was necessary to keep track of two quantities for each of the normal modes: First, the number of quanta of vibrational energy deposited in the excited state for mode k was given by v_k for a given ground vibrational level i_k. Here, k may be any of the 28 normal modes of rhodopsin, $0 < k \leq 28$. Second, the probability for this transition to v_k for a given number of ground- and excited-state quanta in the remaining 27 modes and at a particular excitation wavelength and ground vibrational level i_k was calculated as the complete Boltzmann-weighted, multimode FC product from Eq. 1. A weighted probability for a given transition to v_k is then proportional to the product of the number of quanta of vibrational energy in the excited state, v_k, with the probability for the transition:

$$v_k \cdot \prod_{j=1}^{N} B_{i_j}\frac{\prod_{j=1}^{N}|\langle v_j|i_j\rangle|^2}{\left[\sum_{j=1}^{N}\varepsilon_j(v_j - i_j) + E_{00} - E_{exc}\right]^2 + \Gamma_L^2}$$
$$j = 1, 2, \cdots k \cdots, N-1, N. \quad (3)$$

A sum of weighted probabilities for all possible values of v_k for mode k was then determined at all values of i_k, $v_{j\neq k}$, and $i_{j\neq k}$, and normalized by the sum of total weighted probabilities for all modes. The resulting normalized, weighted probability (or energy distribution) for each mode reflects the relative contribution any given mode makes to the overall absorption cross section at a particular excitation wavelength. In this manner, we quantitatively determined the nature of energy partitioning to all FC active modes upon photoexcitation as a function of incident wavelength.

Absorption spectrum calculation

The development of time-dependent (Heller et al., 1982; Lee and Heller, 1979) and time-correlator (Page, 1991; Page and Tonks, 1981) methods have made the calculation of multimode absorption spectra with thermal ground-state excitation very efficient. A full absorption spectrum for the 28-mode rhodopsin system can be completed in less than 1 min. Unfortunately, the partitioning of mode-specific excitation is hidden in these calculations, necessitating a return to the earlier method based on classic perturbation theory. Because this calculation scales as $(v_j i_j)^N$, the number of terms in σ_A for rhodopsin is truly formidable and the calculation time for 28 modes with thermal occupation is reasonable with a single processor only when some

approximations are made. For example, it was necessary to utilize cutoff values in our thermalized algorithm to truncate the sum at an appropriate level. Two different cutoff values were implemented: a multimode cutoff value was compared to the calculated Boltzmann-weighted, FC multimode product $\prod_{j=1}^{N} B_{i_j}|\langle v_j|i_j\rangle|^2$ for given values of i_j and v_j to determine whether the term should be included in σ_A, and a Boltzmann cutoff was used to determine the uppermost vibrational ground-state level based on the population. Inclusion of these cutoff values was necessary to make the calculation tractable; out of a possible $\sim 10^{95}$ total terms for σ_A (50 ground and 50 excited-state levels), our algorithm calculated only the most significant $\sim 10^9$ terms for a reasonable thermalized absorption spectrum. We found that over 90% of the true time-dependent calculation was recovered when only those terms in which the Boltzmann weighted, Franck-Condon product $\prod_{j=1}^{N} B_{i_j}|\langle v_j|i_j\rangle|^2$ was $>10^{-11}$ and the Boltzmann term B_{i_j} was $>10^{-6}$ were included, and this calculation required 95 h on a 1.4-GHz Pentium 4 processor.

RESULTS

Results from our sum-over-states calculation are compared in Fig. 4 to analogous results from a time-dependent calculation using the parameters in Table 1. The top panel (*A*) displays absorption spectra calculated at $T \sim 0$ K with only homogeneous broadening. These unthermalized spectra calculated via either the time-dependent or sum-over-states method are identical, verifying that our algorithm gives accurate results at 0 K. The middle panel (*B*) presents fully thermalized $T = 298$ K spectra from sum-over-states and time-dependent calculations in which only homogeneous broadening has been considered. The integrated area of the curve resulting from the sum-over-states calculation is within 90% of the integrated area of the time-dependent calculation. In addition, the spectral features are identical, verifying that our algorithm provides accurate results for 298-K calculations. As more terms were included in the sum-over-states calculation, the resulting spectra continued to converge to the time-dependent result with a dramatic increase in computational time. The spectrum shown in Fig. 4 *B* required 95 h of continuous calculation. Achieving further significant improvement of the spectrum would require an unreasonable amount of computation time and was not explored. The bottom panel (*C*) of Fig. 4 presents calculated spectra at $T =$ 298 K with both homogeneous and inhomogeous broadening. Again, the spectrum resulting from a thermalized sum-over-states calculation is within 90% of the spectrum from a time-dependent calculation.

An experimental absorption spectrum of rhodopsin is also presented in the bottom panel of Fig. 4 as the dotted curve. Calculated spectra do not reproduce the full experimental peak height as well as the blue edge of the curve. These differences are partly due to the use of a Lorentzian homogeneous broadening factor. When a Gaussian factor

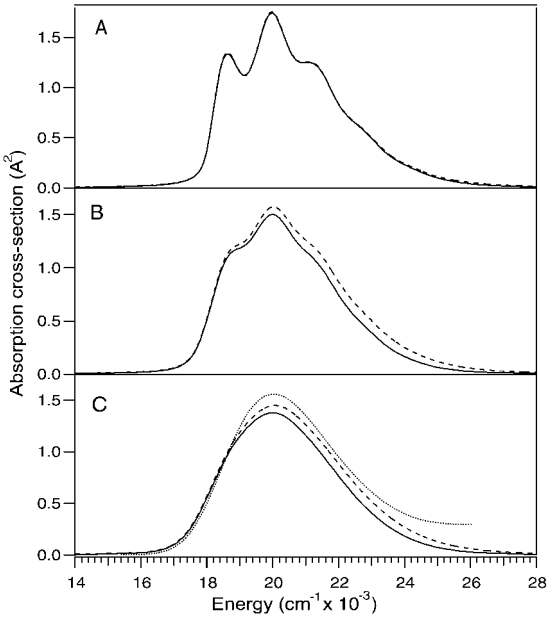

FIGURE 4 Comparison of results from sum-over-states and time-dependent calculations of the rhodopsin absorption. (*A*) Unthermalized sum-over-states (*solid*) and time-dependent (*dashed*) calculations with $\Gamma_L = 165$ cm^{-1}, $\theta_{inh} = 0$; (*B*) fully thermalized (298 K) sum-over-states (*solid*) and time-dependent (*dashed*) calculations with $\Gamma_L = 165$ cm^{-1}, $\theta_{inh} = 0$; and (*C*) fully thermalized (298 K) sum-over-states (*solid*) and time-dependent (*dashed*) calculations with $\Gamma_L = 165$ cm^{-1}, $\theta_{inh} = 522$ cm^{-1}. The experimental absorption spectrum is shown in *C* as a dotted curve. All calculations use $E_{00} = 18130$ cm^{-1}, $n = 1.33$, $M = 2.114$ Å, and mode frequencies and Δ's listed in Table 1.

TABLE 1 Normal modes and excited-state displacements for rhodopsin

Mode (cm^{-1})	Normal mode assignment	Δ (unitless)
93	Skeletal torsion	0.90
131	Skeletal torsion	1.61
246	CCC bend	0.95
260	C_{10}–C_{13} A_2 skeletal torsion	0.94
320	Skeletal torsion	0.73
410		0.31
446		0.30
568	C_{11}=C_{12} A_2 torsion	0.30
793	Ionone ring vibration	0.20
843	C_7=C_8 HOOP + 10H wag	0.29
970	C_{11}=C_{12} A_2 HOOP–C_{11}=C_{12} torsion	0.57
997	13-methyl rock	0.17
1018	9-methyl rock	0.45
1098	C_{10}–C_{11} stretch	0.17
1190	C_{14}–C_{15} stretch	0.30
1214	C_8–C_9 stretch	0.45
1238	C_{12}–C_{13} stretch + 14H rock	0.46
1268	11H–12H rock	0.48
1318		0.20
1357		0.24
1389	13-methyl deform	0.17
1435		0.22
1451		0.17
1548	C=C in phase stretch	0.88
1578	C=C stretch	0.20
1606	C=C stretch	0.31
1635	C=C stretch	0.23
1655	C=N stretch	0.26

From Lin et al. (1998). HOOP, hydrogen out-of-plane.

is used instead of a Lorentzian in the time-dependent calculation, the resulting spectrum is identical to the experimental absorption curve in all spectral regions with the exception of the blue edge. The presence of other excited states on the blue edge of the absorption is the most likely cause for deviation in this region (Birge et al., 1985). The sum-over-states algorithm is intrinsically Lorentzian broadened; therefore a similar comparison could not be performed without major modification of the sum-over-states equation. However, the similarity between the time-dependent and sum-over-states results with Lorentzian broadening supports the use of Eq. 1 to obtain mode-specific information about the distribution of excitation energy.

Mode-specific energy distribution

Normalized, weighted energy distributions were calculated for each mode as a function of incident wavelength for the unthermalized and fully thermalized absorption spectra in Fig. 4 and this result is presented in Fig. 5. The low-frequency modes with large Δ's dominate both the unthermalized and thermalized absorption spectra at any given wavelength; the three lowest-frequency modes of 93, 131, and 246 cm^{-1} contribute 40–72% to the total absorption cross section between 450 and 570 nm. The ethylenic at 1548 cm^{-1} also contributes significantly to the absorption band, but this contribution is strongly wavelength dependent, ranging from 1 to 8% (thermalized) and 3 to 13% (unthermalized), with the largest contribution made when the excitation energy exceeds the ethylenic $0 \rightarrow 1$ and $0 \rightarrow 2$ transitions. Other high-frequency modes contribute $<2\%$ each. The main difference between the normalized, weighted energy distributions calculated at 0 and 298 K is the contribution of low-frequency modes to the overall absorption cross section. The increase in the number of initially populated low-frequency ground-state modes in the thermalized calculation results in an increase in the total number of transitions to the excited state by these low-frequency modes.

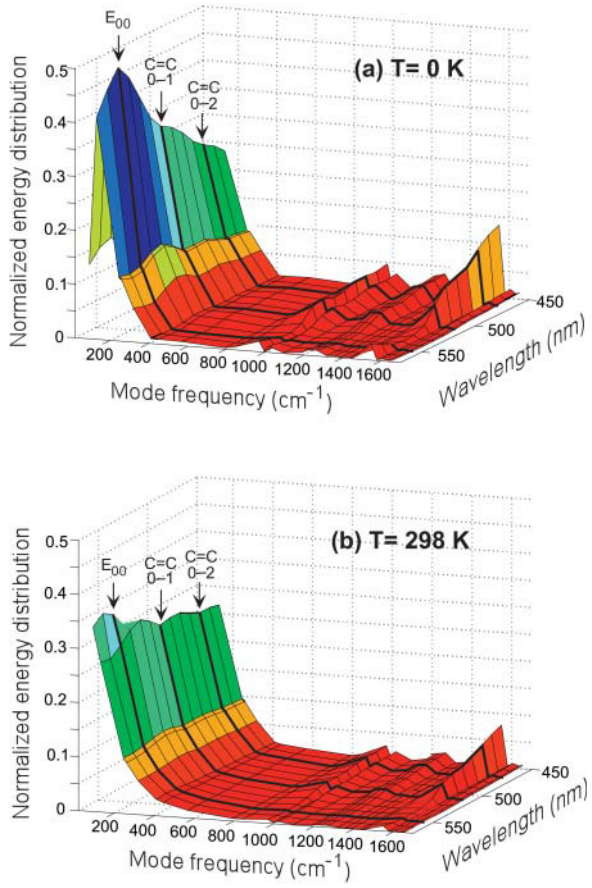

FIGURE 5 Contribution of the Franck-Condon active modes to σ_{abs} as a function of incident wavelength. (*a*) Unthermalized ($T = 0$ K) and (*b*) thermalized ($T = 298$ K) distributions. The normalized, weighted distributions were calculated using Eq. 1 with $E_{00} = 18{,}130$ cm^{-1}, $n = 1.33$, $M = 2.114$ Å, $\Gamma_L = 165$ cm^{-1}, $\theta_{inh} = 0$, and mode frequencies and Δ's listed in Table 1.

The 28-dimensional potential energy surface was reduced to a two-dimensional surface by separating the 28 modes into various partitions of ''reactive'' and ''unreactive'' coordinates. Table 1 lists normal mode assignments for each of the 28 modes in rhodopsin. In one calculation, the localized reactive coordinate consisted of localized torsions at 260, 568, and 970 cm^{-1} whereas the unreactive coordinate contained the remaining 25 modes. In a second calculation, the reactive coordinate consisted of delocalized and localized torsions (93, 131, 246, 260, 320, 568, 970 cm^{-1}) as well as unassigned low-frequency modes (410 and 446 cm^{-1}). This second grouping is referred to as the delocalized reaction coordinate. The normalized energy distributions in the reactive and unreactive sets of coordinates are presented in Fig. 6. When the reactive coordinate is described by only three localized torsions, the distribution of energy into reactive and unreactive degrees of freedom is nearly wavelength independent. Inclusion of delocalized torsions in the reactive dimension causes a change in partitioning of energy as a function of wavelength; the contribution of the reactive coordinate is more significant in the red region of the absorption than in the blue region.

Quantum yield prediction from LZ model

Once the multimode contribution to σ_A is reduced to two dimensions, we can calculate the wavelength dependence of the quantum yield, ϕ_λ, using a simple Landau Zener model. Fig. 1 presents a two-dimensional schematic of the internal conversion process for rhodopsin in which absorption of a photon deposits energy (E_{xs}) to the excited-state wavepacket that evolves along reactive and unreactive coordinates before curve crossing to form product. In this model, the quantum yield for isomerization is given as $\phi_\lambda = e^{-k/v}$ where k depends on the energy difference and slopes of the ground and excited-state potential energy surfaces and

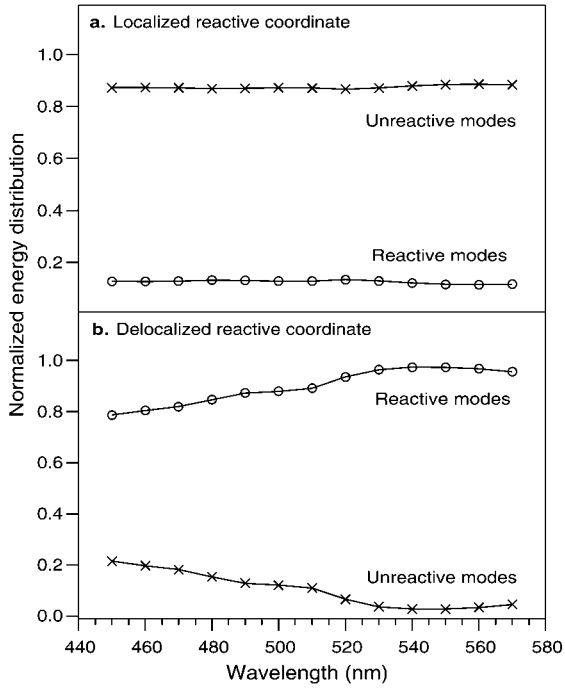

FIGURE 6 Normalized, weighted energy distribution in reactive and unreactive rhodopsin coordinates as a function of excitation wavelength. (*a*) Results for localized reactive coordinate (260, 568, 970 cm^{-1}) in which the reactive pathway is defined by the sum of three localized torsional modes (○) and the unreactive pathway consists of the remaining 25 modes (×). (*b*) Results for delocalized reactive coordinate (93, 131, 246, 260, 320, 410, 446, 568, 970 cm^{-1}) in which the reactive pathway is made up of nine delocalized torsional modes (○) and the unreactive coordinate consists of the remaining 19 modes (×).

v is the wavepacket velocity at the crossing region. Our key hypothesis is that the wavelength dependence of the quantum yield arises because v is proportional to the square root of excess energy deposited into reactive modes. We can rewrite the LZ equation as $\phi_\lambda = e^{-k'/\sqrt{E_{rxt}}}$ where k' now has an additional factor resulting from the conversion of velocity to energy. E_{rxt} is the excess energy along the reaction coordinate, which is equal to the total excess energy (E_{xs}) times the percentage of energy distributed to the reactive modes. The total excess energy E_{xs} is given as

$$E_{xs} = E_{phot} - \left[E_{00} - \sum_{i=1}^{FC}\left(\frac{h\nu_i}{e^{h\nu_i/kT} - 1}\right)\right], \qquad (4)$$

where E_{phot} is the photon energy, E_{00} is the energy difference between the lowest vibrational levels of the excited and ground states, and the last term corresponds to the sum of vibrational energies of the Franck-Condon active modes in the ground state at a given temperature. Because the last two terms in E_{xs} are fixed, Eq. 4 can be reduced to $E_{xs} = E_{phot} - E_{00}^{eff}$, where E_{00}^{eff} is defined as the difference between E_{00} and the sum of ground state vibrational energies.

We then utilized both the localized and delocalized coordinate partitioning to calculate the wavelength dependence of ϕ. A critical aspect of these calculations is the choice of E_{00}. Raman intensity analysis suggests a value of 18,130 cm^{-1} (~550 nm) for E_{00} (Lin et al., 1998). An earlier temperature-dependent bleaching study suggested an E_{00} value of ~590 nm (St. George, 1952). In our determination of ϕ_λ/ϕ_{500} we choose the average of the values determined by Raman analysis and temperature-dependence studies (E_{00} = 17,544 cm^{-1}). Using the FC vibrational energy of 862 cm^{-1}, E_{00}^{eff} has a value of 16,682 cm^{-1} (~600 nm) and the resulting value for E_{xs} is then weighted by our result in Fig. 6 to yield E_{rxt} (500 nm) = 2933 cm^{-1} and therefore k' = 23 $cm^{-1/2}$. Values for ϕ_λ/ϕ_{500} based on this value of k' in the LZ equation are presented in Fig. 7. Relative quantum yields when the reaction coordinate consists only of localized torsional modes have a stronger wavelength dependence than experimentally observed. As more delocalized torsional modes are included in the reaction coordinate, however, the resulting ϕ_λ/ϕ_{500} ratios begin to approach the experimental data. When inhomogeneous (full width at half maximum (FWHM) 1230 cm^{-1}) and homogeneous (FWHM 330 cm^{-1}) broadening mechanisms are considered, the value for E_{00}^{eff} is reduced to 15,122 cm^{-1} (660 nm) and this new E_{00}^{eff} combined with a delocalized torsional coordinate yields improved ϕ_λ/ϕ_{500} values. By reducing E_{00}^{eff} to 725 nm, the calculated results are even closer to the experimental data. No further improvement in the calculated quantum yield was achieved with the inclusion of additional modes in the reactive coordinate, such as single-bond stretches and methyl rocks.

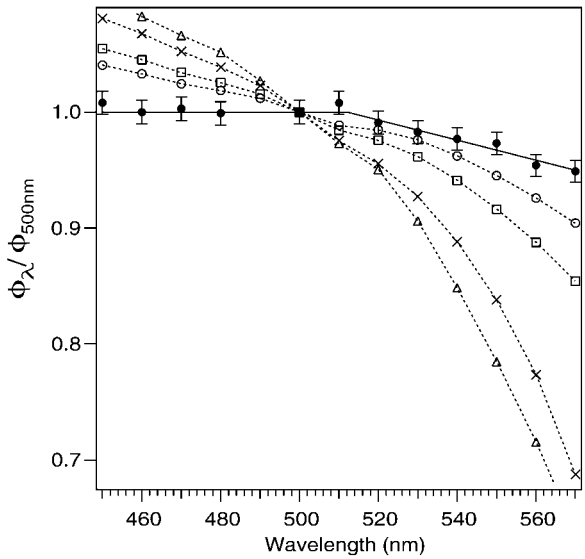

FIGURE 7 Predicted wavelength dependence of the quantum yield. Relative quantum yields for a localized reaction coordinate and E_{00}^{eff} = 600 nm is given (*dashed line*, △). Wavelength dependence of the quantum yield for a delocalized reaction coordinate with E_{00}^{eff} = 600, 660, or 725 nm is given (*dashed line*, ×), (*dashed line*, □); and (*dashed line*, ○), respectively. The experimental result is given (●).

DISCUSSION

We have quantitatively analyzed the mode-specific distribution of energy in the Franck-Condon active modes of rhodopsin through a thermalized sum-over-states calculation. Combined with experimental knowledge of the wavelength dependence of the reaction quantum yield, this analysis allows us to better understand the non-RRKM internal conversion and multidimensional reaction coordinate of rhodopsin. Incorporation of our results into the one-dimensional Landau-Zener picture yields a qualitative understanding of the wavelength dependence of ϕ, while also indicating the need for more sophisticated models.

Nature of the reaction coordinate

The spontaneous excited-state emission spectrum (Kochendoerfer and Mathies, 1996) and reaction quantum yield (Fig. 2) of rhodopsin are both wavelength dependent, providing strong evidence that the *cis*-to-*trans* isomerization occurs before randomization and thermalization of vibrational energy. Recent anti-Stokes Raman data on the primary photoproduct also support this result (Kim and Mathies, 2002). Consistent with the experimental results, our sum-over-states calculation indicates that the distribution of photon energy among the FC accessible vibrational modes varies by as much as 25% as the incident wavelength is changed. Specifically, the high-frequency modes make a significantly larger contribution to the overall absorption cross section with blue excitation; in contrast, low-frequency modes become more dominant in the red region. The strong wavelength dependence of the ethylenic mode is consistent with the picture that vibrational progression in this mode dominates the breadth of the absorption spectrum at energies higher than E_{00} (Loppnow and Mathies, 1988; Warshel and Karplus, 1974).

We have quantified the energy distribution in the 28 Franck-Condon modes as a function of excess energy using an E_{00}^{eff} value of 16,682 cm^{-1} (600 nm). As the photon energy is increased beyond E_{00}^{eff}, absorption to the S_1 state occurs and excess energy is primarily deposited in low-frequency modes. The relative distribution of energy in the low-frequency modes remains essentially unchanged as the photon energy increases. As the photon wavelength decreases from 570 to 530 nm, there is <1% change in probability for absorption by low-frequency modes (<500 cm^{-1}). When the excitation wavelength is 520 nm and lower, however, a different trend emerges in which the relative probability for absorption by the low-frequency modes decreases with increasing photon energy; the relative distribution of excess energy in the low-frequency modes is decreased by 15% with 450-nm excitation relative to a 520-nm photon. This occurs because absorption by the ethylenic mode becomes more significant once the $0 \rightarrow 1$ transition becomes energetically accessible at ~510 nm.

Our model using two partitions of the torsional modes helps elucidate the degrees of freedom that contribute to the photoisomerization, and explains the transition at 500 nm from a wavelength-dependent to flat quantum yield. The reactive pathway is likely dominated by torsional modes. Localized torsions that contribute to the reaction coordinate have been identified as the 970 cm^{-1} C_{11}=C_{12} hydrogen out-of-plane (HOOP) mode (Eyring et al., 1982; Garavelli et al., 1999b), the 568 cm^{-1} C_{11}=C_{12} torsion (Lin et al., 1998; Loppnow and Mathies, 1988; Birge et al., 1982), and the 260 cm^{-1} C_{10}~C_{13} skeletal torsion (Lin et al., 1998). However, a reaction coordinate consisting solely of these three localized torsions results in a much stronger wavelength dependence in the 450–570 nm region than observed. The strong wavelength dependence results because the excess energy in these modes depends only on the absorbed photon energy. When other delocalized low-frequency torsions are included in the calculation, these additional modes modulate the resulting distribution of excess energy along the reactive coordinate and yield a result that is more consistent with our measured wavelength dependence of ϕ_λ/ϕ_{500} as shown in Fig. 7. The fact that the distribution of energy along the reactive coordinate is flat over the range 520–570 nm leads to a decline in the calculated quantum yield over the same wavelength region due to the decline in photon energy. This is consistent with the experimentally observed variation of quantum yield and our basic hypothesis on the role of excess energy in the LZ isomerization process. In the 510–450 nm region, however, the increase in photon energy is offset by the fact that less of the available energy is deposited into the reactive coordinates; consequently, there is a less pronounced effect of incident wavelength on the calculated quantum yield in this spectral region. This finding is qualitatively consistent with our experimental result in which the quantum yield becomes wavelength independent in the blue region.

The simple comparison of the wavelength dependence of the energy distribution for the two different reaction coordinates illustrates the mode-specific nature of the multidimensional reactive pathway. A reaction coordinate defined solely by three localized torsional motions about the C_{11}=C_{12} bond is inconsistent with experimental observation. However, when the reaction coordinate is expanded and consists of both localized and delocalized torsions, there is qualitative agreement between the calculated wavelength dependence of the energy distribution and the observed ϕ_λ/ϕ_{500}. Therefore, it appears that delocalized torsional modes must play a significant role in the reaction coordinate.

We have modeled the wavelength dependence of the quantum yield using the LZ formula and find qualitative agreement with our experimental results, especially when inhomogenous and homogeneous broadening of the absorption process are considered. Fig. 7 shows that the calculated quantum yield ($E_{00}^{\text{eff}} = 660$ nm) increases by 18% with a change in excitation wavelength from 570 to 500 nm, but only increases by 5% as the photon energy is further increased to $\lambda_{\text{exc}} = 450$ nm; the predicted change in quantum

yield between 570 and 500 nm is ~4 times the change predicted between 500 and 450 nm. The relative change in quantum yield is similar to what we observe experimentally; the change in quantum yield observed between 570 and 500 nm (5%) is at least 5 times greater than the change observed between 500 and 450 nm (<1%). When E_{00}^{eff} is further reduced to 725 nm, the calculated ratio ϕ_λ/ϕ_{500} begins to quantitatively approach the experimental result. Overall, these calculations allow us to understand why the quantum yield for rhodopsin is wavelength dependent in red but constant in blue spectral regions.

Because the excited-state isomerization dynamics in rhodopsin are influenced by the initially prepared state, a direct probe of the mode-specific nature of the reaction coordinate should be possible. Our calculation indicates that most of the excess energy is localized in low-frequency torsional motion, especially when the incident wavelength is red (>520 nm). This suggests that it should be possible to selectively excite reactive torsional modes using, for example, an infrared pump to study the effect of mode-specific preparation on the isomerization quantum yield and dynamics, as observed for the unrelaxed photoisomerization of gas-phase *trans*-stilbene (Syage et al., 1984).

Protein versus solution photochemistry

The binding pocket environment significantly enhances the photoisomerization reaction in opsin relative to a solvent such as methanol. For example, the reaction quantum yield for the 11-*cis* retinal protonated Schiff base is ~0.2 and independent of wavelength in at least four different solvents (Becker and Freedman, 1985). In addition, the product formation time of ~10 ps in methanol (Kandori et al., 1995) is much slower than that for the chromophore in protein (200 fs). These differences are consistent with the idea that the protein-binding pocket accelerates the initial torsional dynamics of the chromophore. A comparison of the Raman spectra of the chromophore in methanol and in rhodopsin reveals that a number of the low-wavenumber reactive modes, namely the 11=12 A_2 HOOP at 970 cm^{-1} and C_{10}–C_{13} A_2 skeletal torsion at 260 cm^{-1}, have significantly greater Raman intensity in the protein (Lin et al., 1998). These larger intensities indicate steeper excited-state slopes along these modes for the protein-bound chromophore, revealing the mechanistic reason for the more efficient isomerization reaction in the protein.

Limitations of the LZ model

Not surprisingly, the LZ model used here does not yield quantitative agreement with experiment. A central assumption in our calculation is of constant nuclear velocity, or that energy remains localized in each of the FC modes on the excited state. Because our calculation yields relative quantum yields that have a greater wavelength dependence than what is experimentally observed, it is likely that some, but not complete, IVR occurs before curve crossing, and the difference between calculated and measured quantum yields may reflect the extent of IVR on S_1. Low-frequency reactive modes are likely to be highly anharmonic and therefore play a significant role in such IVR. Other simplifications are inherent in the LZ model, such as the use of a classical one-dimensional reaction coordinate and an unchanging difference in slopes of the diabatic surfaces in the crossing region. Several studies have addressed these limitations and expanded the LZ model to incorporate a multidimensional surface (Zhu et al., 1997) as well as quantum mechanical wavepacket dynamics (Henriksen, 1992) and stochastic energy fluctuations (Kayanuma, 1984). Other models, such as the nonequilibrium golden rule formula (Coalson et al., 1994; Cho and Silbey, 1995) or Redfield theory (Jean, 1996), may also be used to quantitate the rapid, unrelaxed internal conversion process in rhodopsin. More recent ab initio calculations (Garavelli et al., 1999a; Garavelli et al., 1998; Vreven et al., 1997; Ben-Nun and Martinez, 1998) have explored the idea that the *cis*-to-*trans* curve crossing process involves true, as opposed to weakly avoided, surface crossings (Bonacic-Koutecky et al., 1984). These and other quantum calculations (Hahn and Stock, 2000; Molteni et al., 1999; La Penna et al., 1998; Ben-Nun and Martinez, 1999) provide a multidimensional picture of the ultrafast isomerization reaction that builds upon the intuitive picture provided by the LZ model. It will be interesting to see how well these more sophisticated computational approaches are able to reproduce the wavelength-dependent quantum yield observed for rhodopsin.

SUMMARY

The ultrafast isomerization reaction in rhodopsin is a unique example of condensed-phase non-RRKM photochemistry because reactive internal conversion occurs before the excited state is vibronically relaxed. One advantage of such nonstationary-state dynamics is that excess photon energy (E_{xs}) likely remains localized in the FC active modes during the photochemical reaction (see Fig. 1), thereby enhancing the isomerization yield. Our calculation of the distribution of energy among the FC active modes as a function of incident wavelength thus provides a useful tool for probing the mode-specific nature of the multidimensional reaction coordinate. Specifically, comparison of the distribution of excess energy with the wavelength-dependent reaction quantum yield allows us to determine which of rhodopsin's 28 FC active modes may be significant contributors to the overall isomerization coordinate. This comparison reveals that at least nine delocalized torsional modes are likely integral components of the reactive pathway, and more generally demonstrates that the mode-specific excited-state calculation

developed here may be a useful tool for understanding other fast condensed phase photochemical and photobiological reactions.

We thank David McCamant for helpful discussions and Larry Shiow and Ziad Ganim for expert rhodopsin preparation.

This work was supported by a grant from the National Institutes of Health (EY-02051)

REFERENCES

Bakker, H. J. 1993. Effect of intermolecular interactions on vibrational-energy transfer in the liquid phase. *J. Chem. Phys.* 98:8496–8506.

Becker, R. S., and K. Freedman. 1985. A comprehensive investigation of the mechanism and photophysics of isomerization of a protonated and unprotonated schiff base of 11-cis-retinal. *J. Am. Chem. Soc.* 107:1477–1485.

Ben-Nun, M., and T. J. Martinez. 1998. Electronic energy funnels in cis-trans photoisomerization of retinal protonated Schiff vase. *J. Phys. Chem. A.* 102:9607–9617.

Ben-Nun, M., and T. J. Martinez. 1999. Electronic absorption and resonance Raman spectroscopy from ab initio quantum molecular dynamics. *J. Phys. Chem. A.* 103:10517–10527.

Birge, R., D. Bocian, and L. Hubbard. 1982. Origins of inhomogeneous broadening in the vibronic spectra of visual chromophores and visual pigments. *J. Am. Chem. Soc.* 104:1196–1207.

Birge, R. R., L. P. Murray, B. M. Pierce, H. Akita, V. Balogh-Nair, L. A. Findsen, and K. Nakanishi. 1985. Two-photon spectroscopy of locked-11-cis-rhodopsin: Evidence for a protonated Schiff base in a neutral protein binding site. *Proc. Natl. Acad. Sci. USA.* 82:4117–4121.

Bonacic-Koutecky, V., J. Kohler, and J. Michl. 1984. Prediction of structural and environmental effects on the S_1-S_0 energy gap and jump probability in double-bond cis-trans photoisomerization. A general rule. *Chem. Phys. Lett.* 104:440–442.

Bunker, D. L., and W. L. Hase. 1973. On non-RRKM unimolecular kinetics: Molecules in general, and CH3NC in particular. *J. Chem. Phys.* 59:4621–4632.

Cho, M., and R. J. Silbey. 1995. Nonequilibrium photoinduced electron transfer. *J. Chem. Phys.* 103:595–606.

Coalson, R. D., D. G. Evans, and A. Nitzan. 1994. A nonequilibrium golden rule formula for electronic state populations in nonadiabatically coupled systems. *J. Chem. Phys.* 101:436–448.

Dartnall, H. 1968. The photosensitivities of visual pigments in the presence of hydroxylamine. *Vision Res.* 8:339–358.

Diau, E. W., J. L. Herek, Z. H. Kim, and A. H. Zewail. 1998. Femtosecond activation of reactions and the concept of nonergodic molecules. *Science.* 279:847–851.

Elsaesser, T., and W. Kaiser. 1991. Vibrational and vibronic relaxation of large polyatomic molecules in liquids. *In* Annual Review Physical Chemistry. H. L. Strauss, editor. Annual Reviews, Inc., Palo Alto, CA. 83–107.

Eyring, G., B. Curry, A. Broek, J. Lugtenburg, and R. Mathies. 1982. Assignment and interpretation of hydrogen out-of-plane vibrations in the resonance Raman spectra of rhodopsin and bathorhodopsin. *Biochemistry.* 21:384–393.

Frost, W. 1973. Theory of Unimolecular Reactions. Academic Press, New York.

Garavelli, M., F. Bernardi, M. A. Robb, and M. Olivucci. 1999a. The short-chain acroleiniminium and pentadieniminium cations: towards a model for retinal photoisomerization. A CASSCF/PT2 study. *J. Mol. Struc. Theochem.* 463:59–64.

Garavelli, M., F. Negri, and M. Olivucci. 1999b. Initial excited-state relaxation of the isolated 11-cis protonated Schiff base of retinal: evidence for in-plane motion from ab initio quantum chemical simulation of the resonance Raman spectrum. *J. Am. Chem. Soc.* 121:1023–1029.

Garavelli, M., T. Vreven, P. Celani, F. Bernardi, M. A. Robb, and M. Olivucci. 1998. Photoisomerization path for a realistic retinal chromophore model: the nonatetraeniminium cation. *J. Am. Chem. Soc.* 120:1285–1288.

Hahn, S., and G. Stock. 2000. Quantum-mechanical modeling of the femtosecond isomerization in rhodopsin. *J. Phys. Chem. B.* 104:1146–1149.

Heller, E. J., R. L. Sundberg, and D. Tannor. 1982. Simple aspects of Raman scattering. *J. Phys. Chem.* 86:1822–1833.

Henriksen, N. E. 1992. Gaussian wavepacket dynamics and the Landau-Zener model for non-adiabatic transitons. *Chem. Phys. Lett.* 197:620–625.

Hurley, J. B., T. G. Ebrey, B. Honig, and M. Ottolenghi. 1977. Temperature and wavelength effects on the photochemistry of rhodopsin, isorhodopsin, bacteriorhodopsin and their photoproducts. *Nature.* 270:540–542.

Jean, J. M. 1996. Vibrational coherence effects on electronic curve crossing. *J. Chem. Phys.* 104:5638–5646.

Kandori, H., Y. Katsuta, M. Ito, and H. Sasabe. 1995. Femtosecond fluorescence study of the rhodopsin chromophore in solution. *J. Am. Chem. Soc.* 117:2669–2670.

Kayanuma, Y. 1984. Nonadiabatic transitions in level crossing with energy fluctuations. I. Analytical investigations. *J. Phys. Soc. Jap.* 53:108–117.

Kim, J. E., and R. A. Mathies. 2002. Anti-Stokes Raman study of vibrational cooling dynamics in the primary photochemistry of rhodopsin. *J. Phys. Chem. A.* 106:8508–8515.

Kim, J. E., M. J. Tauber, and R. A. Mathies. 2001. Wavelength dependent cis-trans isomerization in vision. *Biochemistry.* 40:13774–13778.

Kim, S. K., J. Guo, J. S. Baskin, and A. H. Zewail. 1996. Femtosecond chemically activated reactions: concept of nonstatistical activation at high thermal energies. *J. Phys. Chem.* 100:9202–9205.

Kochendoerfer, G. G., and R. A. Mathies. 1995. Ultrafast spectroscopy of rhodopsins - photochemistry at its best. *Isr. J. Chem.* 35:211–226.

Kochendoerfer, G. G., and R. A. Mathies. 1996. Spontaneous emission study of the femtosecond isomerization dynamics of rhodopsin. *J. Phys. Chem.* 100:14526–14532.

La Penna, G., F. Buda, A. Bifone, and J. J. M. de Groot. 1998. The transition state in the isomerization of rhodopsin. *Chem. Phys. Lett.* 294:447–453.

Landau, L. D. 1932. Zur theorie der energieübertragung. *Phys. Z. Sowjet*: 2:46–51.

Lax, M. 1952. The Franck-Condon principle and its application to crystals. *J. Chem. Phys.* 20:1752–1760.

Lee, I., W. Chen, Y. Chung, and P. Cheng. 2000. A direct observation of non-RRKM behavior in femtosecond photophysically activated reactions. *J. Phys. Chem. A.* 104:10595–10599.

Lee, S. Y., and E. J. Heller. 1979. Time-dependent theory of Raman scattering. *J. Chem. Phys.* 71:4777–4788.

Lin, S. W., M. Groesbeek, I. van der Hoef, P. Verdegem, J. Lugtenburg, and R. A. Mathies. 1998. Vibrational assignment of torsional normal modes of rhodopsin: probing excited-state isomerization dynamics along the reactive C_{11}=C_{12} torsional coordinate. *J. Phys. Chem. B.* 102: 2787–2806.

Loppnow, G. R., and R. A. Mathies. 1988. Excited state structure and isomerization dynamics of the retinal chromophore in rhodopsin from resonance Raman intensities. *Biophys. J.* 54:35–43.

Manneback, C. 1951. Computation of the intensities of vibrational spectra of electronic bands in diatomic molecules. *Physica.* 17:1001–1010.

Mathies, R., and J. Lugtenburg. 2000. The primary photoreaction of rhodopsin. *In* Handbook of Biological Physics. E. G. Stavenga, W. J. DeGrip, E. N. Pugh Jr., editors. Elsevier Science Press, Leiden, The Netherlands. 55–90.

Mathies, R. A. 1999. Photons, femtoseconds and dipolar interactions: a molecular picture of the primary events in vision. *In* Rhodopsins and Phototransduction. John Wiley and Sons, New York. 70–89.

Molnar, F., M. Ben-Nun, T. J. Martinez, and K. Schulten. 2000. Characterization of a conical intersection between the ground and first excited state for a retinal analog. *J. Mol. Struc. Theochem.* 506:169–178.

Molteni, C., I. Frank, and M. Parrinello. 1999. An excited state density functional theory study of the rhodopsin chromophore. *J. Am. Chem. Soc.* 121:12177–12183.

Myers, A. B., and R. A. Mathies. 1987. Resonance Raman intensities: a probe of excited state structure and dynamics. *In* Biological Applications of Raman Spectroscopy: Resonance Raman Spectra of Polyenes and Aromatics. T. G. Spiro, editor. John Wiley and Sons, New York. 1–58.

Page, J. B. 1991. Many-body approach to the theory of resonance Raman scattering by vibronic systems. *In* Light Scattering in Solids: Recent Results, Including High-Tc Superconductivity. M. Cardona, G. Güntherodt, editors. Springer-Verlag, New York. 17–72.

Page, J. B., and D. L. Tonks. 1981. On the separation of resonance Raman scattering into orders in the time correlator theory. *J. Chem. Phys.* 75:5694–5708.

Sakmar, T. P., S. T. Menon, E. P. Marin, and E. S. Awad. 2002. Rhodopsin: insights from recent structural studies. *Annu. Rev. Biophys. Biomol. Struct.* 31:443–484.

Schoenlein, R. W., L. A. Peteanu, Q. Wang, R. A. Mathies, and C. V. Shank. 1993. Femtosecond dynamics of cis-trans isomerization in a visual pigment analog: isorhodopsin. *J. Phys. Chem.* 97:12087–12092.

St. George, R. C. C.1952. The interplay of light and heat in bleaching rhodopsin. *J. Gen. Phys.* 35:495–517.

Syage, J. A., P. M. Felker, and A. H. Zewail. 1984. Picosecond dynamics and photoisomerization of stilbene in supersonic beams. II. Reaction rates and potential energy surface. *J. Chem. Phys.* 81:4706–4723.

Vreven, T., F. Berhardi, M. Garavelli, M. Olivucci, M. A. Robb, and H. B. Schlegel. 1997. Ab initio photoisomerization dynamics of a simple retinal chromophore model. *J. Am. Chem. Soc.* 119:12687–12688.

Wald, G. 1968. Molecular basis of visual excitation. *Science.* 162:230–239.

Wang, Q., R. W. Schoenlein, L. A. Peteanu, R. A. Mathies, and C. V. Shank. 1994. Vibrationally coherent photochemistry in the femtosecond primary event of vision. *Science.* 266:422–424.

Warshel, A., and M. Karplus. 1974. Calculation of pi-pi* excited state conformations and vibronic structure of retinal and related molecules. *J. Am. Chem. Soc.* 96:5677–5689.

Zener, C. 1932. Non-adiabatic crossing of energy levels. *Proc. Roy. Soc. London A.* 137:696–703.

Zhu, L., A. Widom, and P. M. Champion. 1997. A multidimensional Landau-Zener description of chemical reaction dynamics and vibrational coherences. *J. Chem. Phys.* 107:2859–2871.